Acta Biomaterialia 22 (2015) 59–69

Contents lists available at ScienceDirect

Acta Biomaterialia

journal homepage: www.elsevier.com/locate/actabiomat

Hydrosoluble, UV-crosslinkable and injectable chitosan for patterned cell-laden microgel and rapid transdermal curing hydrogel *in vivo*

Baoqiang Li [a,b,*], Lei Wang [a], Feng Xu [c,d], Xiaomin Gang [a], Utkan Demirci [e], Daqing Wei [a], Ying Li [f,g], Yujie Feng [a], Dechang Jia [a], Yu Zhou [a]

[a] Institute for Advanced Ceramics, State Key Laboratory of Urban Water Resource and Environment, Harbin Institute of Technology, Harbin 150001, PR China
[b] Bio-acoustic MEMS in Medicine Laboratory, Department of Medicine, Division of Biomedical Engineering, Brigham and Women's Hospital, Harvard Medical School, Boston, MA, 02115, USA
[c] MOE Key Laboratory of Biomedical Information Engineering, School of Life Science and Technology, Xi'an Jiaotong University, Xi'an 710049, PR China
[d] Bioinspired Engineering and Biomechanics Center (BEBC), Xi'an Jiaotong University, Xi'an 710049, PR China
[e] Stanford University School of Medicine, Radiology Department, Canary Center at Stanford for Cancer Early Detection, Palo Alto, CA 94304, USA
[f] Sino-Russian Institute of Hard Tissue Development and Regeneration, The Second Affiliated Hospital of Harbin Medical University, Harbin 150001, PR China
[g] Heilongjiang Academy of Medical Sciences, Harbin 150001, PR China

ARTICLE INFO

Article history:
Received 10 November 2014
Received in revised form 16 April 2015
Accepted 19 April 2015
Available online 25 April 2015

Keywords:
Patterned microgels
Injectability
Transdermal photopolymerization
Photolithography
Localized delivery

ABSTRACT

Natural and biodegradable chitosan with unique amino groups has found widespread applications in tissue engineering and drug delivery. However, its applications have been limited by the poor solubility of native chitosan in neutral pH solution, which subsequently fails to achieve cell-laden hydrogel at physiological pH. To address this, we incorporated UV crosslinking ability in chitosan, allowing fabrication of patterned cell-laden and rapid transdermal curing hydrogel *in vivo*. The hydrosoluble, UV crosslinkable and injectable N-methacryloyl chitosan (N-MAC) was synthesized *via* single-step chemoselective N-acylation reaction, which simultaneously endowed chitosan with well solubility in neutral pH solution, UV crosslinkable ability and injectability. The solubility of N-MAC in neutral pH solution increased 2.21-fold with substitution degree increasing from 10.9% to 28.4%. The N-MAC allowed fabrication of cell-laden microgels with on-demand patterns *via* photolithography, and the cell viability in N-MAC hydrogel maintained 96.3 ± 1.3% N-MAC allowed rapid transdermal curing hydrogel *in vivo* within 60 s through minimally invasive clinical surgery. Histological analysis revealed that low-dose UV irradiation hardly induced skin injury and acute inflammatory response disappeared after 7 days. N-MAC would allow rapid, robust and cost-effective fabrication of patterned cell-laden polysaccharide microgels with unique amino groups serving as building blocks for tissue engineering and rapid transdermal curing hydrogel *in vivo* for localized and sustained protein delivery.

1. Introduction

Tissue engineering based on microfabrication, assembly, and *in vitro* culturing of cell-laden three dimensional (3D) extracellular matrix (ECM) analogs has been developed for several decades [1–6]. Serving as cell-laden 3D ECM analogs, patterned cell-laden microscale hydrogels (microgels) could accurately replicate the heterogeneous nature of native cellular environments. For regenerating complex tissues and organs *in vitro*, one reliable strategy is fabrication of cell-laden microgels serving as building blocks, which are then assembled to form complex artificial micro-tissues with specific physiological function *via* bottom-up tissue engineering [7,8]. Various microfabrication 3D patterned cell-laden building blocks with natural and/or synthetic polymer have been widely adopted, such as photolithography [9–11], micromolding [12] and bioprinting [13,14]. So far, the versatile and efficient cell-friendly photolithography allows fabrication of patterned building blocks with advantages of high precision, short time and low costs especially in fabrication of 3D patterned building blocks [15–17]. Various cells were seeded on patterned azido-chitosan hydrogel fabricated by UV lithography, such as cell spheroid microarrays of Hep G2 and NIH/3T3 [18], patterned cardiac fibroblast, cardiomyocyte and osteoblast microarrays on chitosan surfaces [19]. UV irradiation time for chitosan gelation is usually 5–15 min [20,21], thus these patterned chitosan hydrogels are not

* Corresponding author at: Institute for Advanced Ceramics, State Key Laboratory of Urban Water Resource and Environment, Harbin Institute of Technology, Harbin 150001, PR China.
E-mail address: libq@hit.edu.cn (B. Li).

http://dx.doi.org/10.1016/j.actbio.2015.04.026
1742-7061/

suitable to encapsulate cells during UV irradiation, which fail to mimic *in vivo* cell niche microenvironment for biomedical applications.

Injectable hydrogels with biodegradability have *in situ* formability, which allow an effective and homogeneous encapsulation of drugs/cells in a minimally invasive way. Biocompatible, biodegradable and injectable hydrogels *via* chemical, temperature, pH and UV irradiation triggered gelation have been developed for localized drug delivery with advantages of minimal invasion and tunable release behavior of therapeutic drugs [22,23]. Chitosan is a biodegradable and natural biomaterial with amino groups, which has been widely used in tissue engineering [24], localized drug delivery [25] and injectable hydrogels for cancer therapy [26] owing to its biological properties such as biodegradability by lysozyme, biocompatibility, antibacterial activity and hemostatic ability. Injectable chitosan could undergo thermal or pH triggered gelation and could be enzymatically degraded *in vivo* by lysozyme and chitosanase enzymes. However it usually takes a long gelation time for previously reported injectable chitosan hydrogel, for example, 5–60 min for thermo-sensitive chitosan/β-glycerophosphate hydrogel [27,28] and 60 min for pH-sensitive chitosan/polyacrylamide hydrogel [29]. In addition, the main component in chitosan hydrogel is glycerol phosphate or non-biodegradable polyacrylamide component rather than chitosan, which increases the risk of biological toxicity to surrounding tissues. UV crosslinkable hydrogels allow injection of hydrogel precursor and following rapid curing at desired position in target tissue under mild physiological conditions in a spatiotemporal controlled manner [30,31], avoiding obvious pH or temperature shock in biological tissues while maintaining intrinsic structure and bioactivity of drugs or biomolecules.

There are some challenges associated with chitosan for its applications in tissue engineering and regenerative medicine, such as poor solubility in neutral pH solution and spatiotemporal designability, which subsequently fail to achieve cell-laden hydrogels with controlled architecture and rapid transdermal curing hydrogel *in vivo*. Chitosan is only dissolved in dilute acid aqueous solution, but hardly in water or cell culture medium, which subsequently limits its cell-related applications. To endow chitosan with hydrosoluble ability, various derivatives have been synthesized by chemically grafting with ferulic acid, phosphorylcholine, 4-imidazolecarboxaldehyde and succinic anhydride [32–35]. Furthermore, hydrosoluble chitosan derivatives have been subsequently endowed with UV-crosslinkable ability through covalent linkage with photosensitive components, such as 4-azidobenzoic acid [36], 2-amino ethyl methacrylate [37], or ethylene glycol acrylate methacrylate [38–40]. A water-soluble and UV-crosslinkable chitosan derivative was synthesized by two-step grafting azide and lactose moieties serving as a biological adhesive [36]. Another water-soluble and UV-crosslinkable chitosan derivative was synthesized for supporting neuronal differentiation of encapsulated neural stem cells using two-step chemical modification: synthesis of carboxylmethyl chitosan and subsequent grafting 2-amino ethyl methacrylate on carboxylmethyl chitosan [37]. A UV crosslinkable chitosan was obtained through amidation reaction with EDC/NHS activation between amino groups of chitosan and carboxyl groups of N-methacryloyl glycine [41]. However this chitosan derivative could be dissolved in acetic acid solution instead of water/cell culture medium. Besides, these synthesis protocols normally involve multistep chemical modification, long UV irradiation time for gelation (usually 3–15 min) and coupling agent (EDC/NHS activation) [20,21].

To achieve hydrosoluble, UV crosslinkable and injectable chitosan for patterned cell-laden microgels and rapid transdermal curing hydrogels, we facilely synthesized a hydrosoluble, UV crosslinkable and injectable N-MAC by single-step chemoselective N-acylation between amino group and methacrylic anhydride without using any coupling agents or catalysts. The methacryloyl groups in N-MAC not only allow well solubility in neutral pH solution but also endow it with UV-crosslinkable ability. Patterned cell-laden N-MAC microgels with on-demand regular geometric shapes and complex logos were fabricated *via* UV lithography for tissue engineering. Finally, injectable and rapid transdermal curing N-MAC hydrogels *in vivo* were developed *via* skin-penetrable UV crosslinking strategy within mice subcutaneous space for localized protein delivery.

2. Materials and methods

2.1. Materials

Chitosan (CS, viscosity average molecular weight $M_\eta = 3.4 \times 10^5$, degree of deacetylation = 91.4%) was purchased from Qingdao Hecreat Bio-tech company Ltd. Methacrylic anhydride (MA, 94%), photoinitiator Irgacure 2959 (I2959) and fluorescein isothiocyanate (FITC) labeled dextran were purchased from Sigma–Aldrich. Sodium bicarbonate was supplied by Sinopharm Chemical Reagent Co. Dialysis tubing with molecular weight cut off range 8000–14,000 was supplied by Solarbio (USA).

2.2. Synthesis of N-MAC

N-MAC was synthesized by single-step chemoselective N-acylation between CS and MA. Typically, MA was added dropwise to 1% (w/v) CS acetic acid solution in which the ratio of anhydride to amino groups was 0.5, 1, 2 and 4, respectively. The reaction was carried out at 60 °C for 6 h. The resulting solution was neutralized and diluted 10-fold with 10% (w/v) sodium bicarbonate solution. The N-MAC was dialyzed against deionized water for 4 days to remove the unreacted reagent. The snow sponge was obtained by lyophilization.

2.3. Characterization of N-MAC

^{1}H NMR was recorded on a Bruker NMR (ADVANCE III, 400 MHz) with D_2O as solvent. The degree of substitution (DS) of N-MAC was calculated by ratio of integrated area of the $H_c \sim H_f$ peaks at 2.52–4.18 ppm to that of the methylene (H_g) peaks at 5.46 and 5.68 ppm according to the Eq. (1).

$$DS = \frac{A_{H(5.5\&5.7)}/2}{A_{H(2.5-4.1)}/5} \times 91.4\% \quad (1)$$

where $A_{H(5.5\ \&\ 5.7)}$, $A_{H(2.5-4.1)}$ were the area of methylene protons peak (H_g) at 5.46 and 5.68 ppm, the ring protons ($H_c \sim H_f$) peak of GlcN residues at 2.52–4.18 ppm respectively. FTIR spectra were recorded on a Perkin-Elmer Spectrum One by the KBr pellets method. The measurement was carried out at 298 K ranging from 500 to 4000 cm^{-1}. X-ray diffraction (D/max-2550, Rigaku) was used to investigate the crystalline of CS and N-MAC. The water solubility of N-MAC was evaluated from turbidity. N-MAC (400 mg) was dissolved in deionized water (10 mL). Following stepwise addition of deionized water, the transmittance of solution was recorded on UV–vis spectrometer using a 1 cm quartz cuvette at 600 nm. Images of N-MAC solution and hydrogels were taken by Canon IXUS 210. ESEM image of N-MAC hydrogel was carried out on a Helios NanoLab 600i with operating voltage of 10.0 kV. The compress testing was carried out with Texture Analyzer TA.XT plus (Stable Micro System, UK) in MARMALADE mode. All tested samples were prepared in cylindrical with height of 10 mm and diameter of 20 mm. The probe (P/0.5) with 5 kg load cell was compressed into the sample to a depth of 2.5 mm at the test-speed of 1 mm/s.

2.4. Rapid gelation and swelling behavior of N-MAC hydrogel

The 15 mg/mL N-MAC solution containing 0.1% (w/w) I2959 was injected into cube PDMS mold with 3 × 3 × 3 mm and irradiated under Omni Cure® S2000 spot curing system (EXFO Inc, Canada) with an intensity of 10 mW/cm^2 for 15 s. The cube shaped N-MAC hydrogel was weighed (S_0) and incubated in 10 mL of PBS solution at 37 °C. At certain interval, the hydrogel was gently taken out and weighed (S_1). The swelling ratio (SR) was determined according to the Eq. (2):

$$SR = S_1/S_0 \times 100\% \quad (2)$$

2.5. N-MAC microgel with spatiotemporal designability

To achieve spatiotemporal microgels, the N-MAC solution with a concentration of 15 mg/mL containing I2959 was added to a container followed by placing photomasks parallel to the container. The photomasks were designed by software (AutoCAD, v2012, Autodesk Inc., CA) including regular geometric pattern (square, circle, concentric ring) and complex microscale logos. Then the resulting solution was irradiated by Omni Cure® S2000 for 15 s. The images of patterned N-MAC microgels were carried out on fluorescence microscope (Nikon Eclipse Ti S). FITC labeled dextran was incorporated for visualization and the matching degree was analyzed by Image Pro 6.

2.6. In vitro cytotoxicity of N-MAC

NIH/3T3 fibroblasts were used to evaluate cell viability. NIH/3T3 cells were cultivated in Dulbecco's Modified Eagles' medium (DMEM, Gibco) supplemented with 10% fetal bovine serum and 1% penicillin–streptomycin and incubated at 37 °C, humidified atmosphere with 5% CO_2. The cytotoxicity of N-MAC solution against NIH/3T3 cells was assessed with cell counting kit-8 (CCK-8, Dojindo Molecular Technologies, US). To prepare the DMEM solution containing N-MAC with concentration of 167.5 g/mL to 670 g/mL, different weights of N-MAC were dissolved in 20 ml DMEM and filtrated by 0.22 μm pore filter for sterilization. Typically, NIH/3T3 cells were seeded in 96-well plates at a cell density of 5 × 10^3 cell per well with 100 μL of medium and cultured for 4 h. The medium was gently refreshed with 100 μL of fresh DMEM medium containing different concentrations of N-MAC. The cells were incubated for another 24 h, 36 and 48 h. Then, 20 μL of CCK-8 assay solution was added into each well. The cells were incubated for another 4 h. The percentages of living cells were calculated by absorbance of Multiskan FC microplate reader (Thermo) with a wavelength of 450 nm. Cells were cultured on tissue culture plastic in the absence of N-MAC solution as the control group. The experiments were conducted in triplicate; and the results presented were the average data with standard deviation.

2.7. Patterned cell-laden N-MAC microgel

The 10 mg/mL DMEM solution of N-MAC containing NIH/3T3 cells was pipetted into the container. The photomask was placed directly on top of container and exposed to UV light (10 mW/cm^2, 15 s). Subsequently, the uncrosslinked prepolymer solution was gently washed away with preheated DMEM. Patterned cell-laden microgels were cultured for 4 h and 2 days in tissue culture plates under standard culture conditions. Cell viability in N-MAC microgel was conducted by LIVE/DEAD Viability/Cytotoxicity Kit (Invitrogen, Life science). The images were taken by a fluorescent microscope (Nikon Eclipse Ti S) and analyzed by Image Pro 6 to calculate the cell viability.

2.8. Rapid transdermal curing N-MAC in vivo

All animal experimental protocols were approved by the local animal care and use regulations (Ethics Committee of Harbin Medical University), and the experiments were carried out under the control of the University's Guidelines for Animal Experimentation. The optical transmission of mice skin was measured using a UV/vis spectrophotometer over the range of 200–370 nm. Skin slices were carefully removed (1.5 × 1.5 cm^2 area) from the backs of 4-week-old mice, attached to a quartz slide, and the transmission spectrum was measured. N-MAC was directly dissolved in PBS to form a homogeneous solution (sterilized by filtration; 0.22 μm pore). All Kunming mice were 5 weeks of age and weighed 25–27 g. The transdermal curing N-MAC hydrogels *in vivo* were carried out *via* subcutaneous injection of mice. After anesthetization, 500 μL of 15 mg/mL N-MAC solution containing I2959 (0.1% w/w) was injected into subcutaneous space of mice back through syringe with 25G needle and then sequentially applied low-dose UV irradiation for 60 s. The *in vivo* inflammatory response of injectable N-MAC hydrogel was determined by histopathological analysis. Tissue samples were removed from euthanized mice at 2, 5, 7 and 10 days and subjected to H&E staining. Hydroxyapatite powders with content of 20% (w/w) were encapsulated in N-MAC hydrogels to visualize hydrogels *in vivo* by noninvasive and feasible Faxitron Specimen Radiography System (Model MX-20, exposure-time of 8 s). For protein localized delivery, 4 mg bovine serum albumin (BSA) was encapsulated in N-MAC hydrogels upon 15 s UV irradiation. The *in vitro* release profile of BSA was monitored by UV–vis spectrophotometry at 595 nm (λ_{max}) in PBS at 37 °C using coomassie protein assay kit.

2.9. Statistical analysis

All the data were expressed as means ± standard deviation of at least triplicate samples. The statistically significant difference was evaluated by Student's T-test, and statistical significance was considered for p value $(^*) < 0.05$: $^*p < 0.05$; $^{**}p < 0.025$; $^{***}p < 0.001$ ($n = 3$).

3. Results and discussion

3.1. Synthesis and characterization of N-MAC

Chitosan is versatile biomedical polymer containing plenty of amino groups and hydroxyl groups. However it is not dissolved in neutral pH solution because of plenty of hydrogen bonds interaction (Fig. 1(A)) and rigid crystalline structure, which limits its application for *in situ* cell encapsulation [42]. To endow chitosan with hydrosoluble ability in neutral pH solution and UV crosslinking ability simultaneously *via* grafting acrylate units on chitosan chains (Fig. 1(A)), we proposed that a single-step chemoselective N-acylation for hydrosoluble, UV-crosslinkable and injectable chitosan since the amino group at C_2 site has much higher activity than the primary hydroxyl group at C_6 site during acylation modification in aqueous media; more than 95% acylation occurred with highly chemoselective N-acylation [43]. Fig. 1(A) shows the schematics of facile synthesis of hydrosoluble, UV-crosslinkable and injectable chitosan between CS and MA without using any coupling agents or catalysts; the incorporated methacryloyl groups act dual roles in allowing hydrosoluble ability and UV crosslinkable ability. N-MAC was synthesized by specifically conjugating methacryloyl groups to amino groups of CS. The chemical structure of N-MAC was confirmed by ^{1}H NMR spectrum (Fig. 1(B)), which clearly shows the signals of vinyl protons at 5.46 and 5.68 ppm (g, 2H, CH_2), methine protons of the GlcN ring at 4.44 ppm

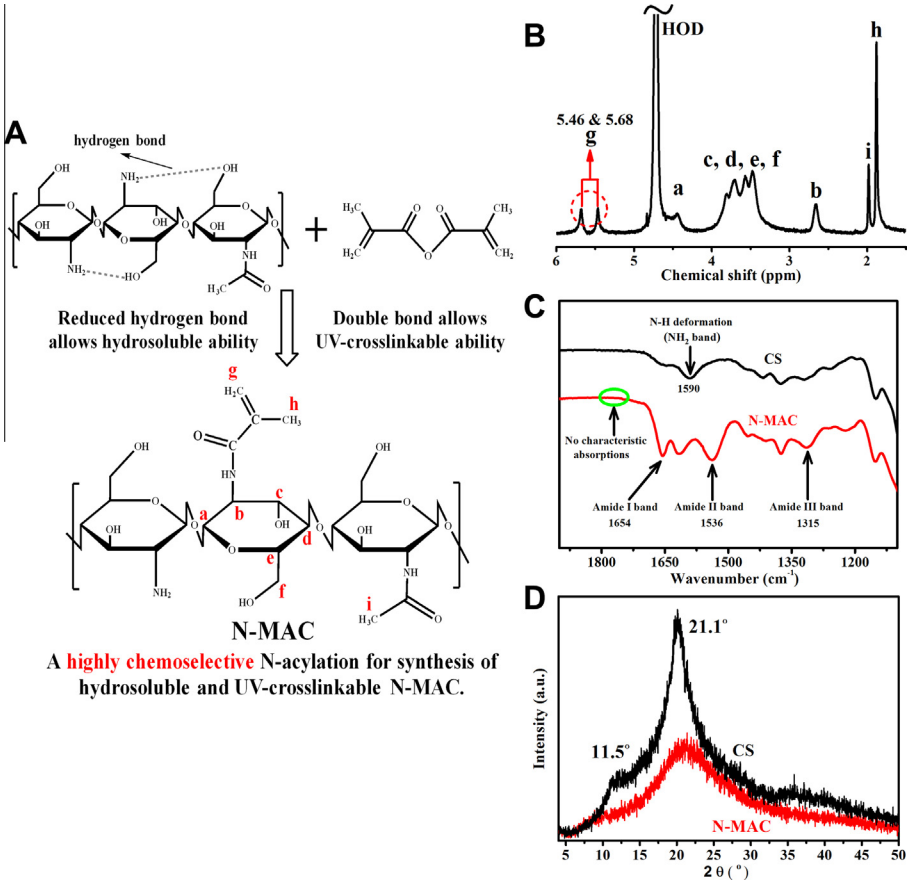

Fig. 1. Synthesis and structure characterization of hydrosoluble, UV-crosslinkable and injectable N-MAC *via* highly chemoselective N-acylation. (A) Highly chemoselective N-acylation scheme between CS and MA. The methacryloyl groups in N-MAC not only allowed CS to be dissolved in cell culture medium facilely due to reduced intra/intermolecular interaction (hydrogen bonds), but also endow CS with UV crosslinkable ability due to the introduced double bond; (B) ^{1}H NMR spectra (400 MHz, D_2O) of N-MAC with DS of 25.8%. The signals of vinyl protons around 5.46 & 5.68 ppm (g, 2H, CH_2), in which the peaks were labeled by red dash ring, confirmed the covalent conjugation of methacryloyl groups to CS and unique chemical structure of N-MAC; (C) FTIR spectra of CS and N-MAC. Newly formed amide absorbance was observed at 1654 cm^{-1}, 1536 cm^{-1} and 1315 cm^{-1}; and no characteristic absorbance of ester groups at 1730–1740 cm^{-1}, which was highlighted by green ring; (D) XRD patterns of CS and N-MAC. The disappeared crystalline peak at $2\theta = 11.5°$ and broad peak at $2\theta = 21.1°$ suggested that large numbers of hydrogen bonds were destroyed and the formation of low crystalline and/or amorphous phase, which improves the solubility of N-MAC in cell culture medium.

(a, 1H, CH), the GlcN ring protons at 3.42–3.95 ppm (c-d-e-f, 5H, CH—CH—CH—CH$_2$), methine protons at 2.66 ppm (b, 1H, CH), methyl protons of N-acetylglucosamine (GlcNAc) at 1.98 ppm (i, 3H, CH_3), methyl protons of methacrylic anhydride residues at 1.88 ppm (h, 3H, CH_3). No chemical shift appeared at 5.5–6.0 ppm in native chitosan NMR spectrum, which was confirmed by other literatures [41,44]; and only vinyl proton would show the chemical shift signals at 5.5–6.0 ppm. ^{1}H NMR spectra result coincided with the schematic structure of N-MAC (Fig. 1(A)), which was attributed to the chemoselective N-acylation between amino groups and MA. FTIR spectra of the CS and N-MAC samples are presented in Fig. 1(C). The peaks for CS at 3355 cm^{-1}, 3294 cm^{-1}, 2867 cm^{-1}, 1590 cm^{-1} and 1151 cm^{-1} indicated O—H stretching, N—H stretching of $-NH_2$, C—H stretching, $-NH_2$ deformation in plan (usually called NH_2 band), and C—O—C bridge symmetric stretching, respectively. Furthermore, several new peaks contributed by the newly formed amide were observed at 1654 cm^{-1}, 1536 cm^{-1} and 1315 cm^{-1}, corresponding to amide I band (C=O stretching), amide II band (N—H deformation and C—N stretching) and amide III band in the spectrum of N-MAC. In addition, there were no characteristic absorptions of ester groups at 1730–1740 cm^{-1} (theoretical ester carbonyl groups, which were highlighted by green ring) in the spectra of N-MAC, which indicated that the esterification reaction between hydroxyl groups ($-$OH) of CS and anhydride groups of MA was avoided. All the above results further confirmed the formation of amide linkage between the methacrylate group and the amino groups. Fig. 1(D) presents XRD patterns of CS and N-MAC. The CS exhibited sharp diffraction peaks at $2\theta = 11.5°$ and 21.1°, which were typical fingerprints of semi-crystalline chitosan [45]. However, the peak at $2\theta = 11.5°$ disappeared and the low intensity peak at $2\theta = 21.1°$ became a relative obtuse and broad. It suggested that large amounts of hydrogen bond between hydroxyl groups ($-$OH) and amino groups ($-NH_2$) in CS intra/intermolecular were destroyed through chemoselective N-acylation, thus forming low crystalline and/or amorphous phase.

DS was a key parameter to determine the solubility of N-MAC and crosslinking density of N-MAC hydrogel, which strongly depended on molar ratio of MA to CS. N-MAC with different DS were synthesized by varying molar ratios of anhydride to amino groups. The DS of N-MAC was 10.9%, 19.9%, 25.8% and 28.4% corresponding to the anhydride to amino groups' molar feed ratios of 0.5, 1, 2 and 4, respectively (Fig. 2(A)). The DS was positively correlated to the ratio of MA used in acylation reaction, which could be accurately controlled by adjusting the ratio of anhydride to amino groups. The solubility of N-MAC in neutral pH solution was critical to encapsulate pH-sensitive proteins, bioactive ligand and cells in hydrogel *via* UV crosslinking and to maintain their bioactivity. Fig. 2(B) shows that the solubility of N-MAC in neutral pH solution increased from 8.6 to 27.6 mg/mL (2.21-fold) with DS

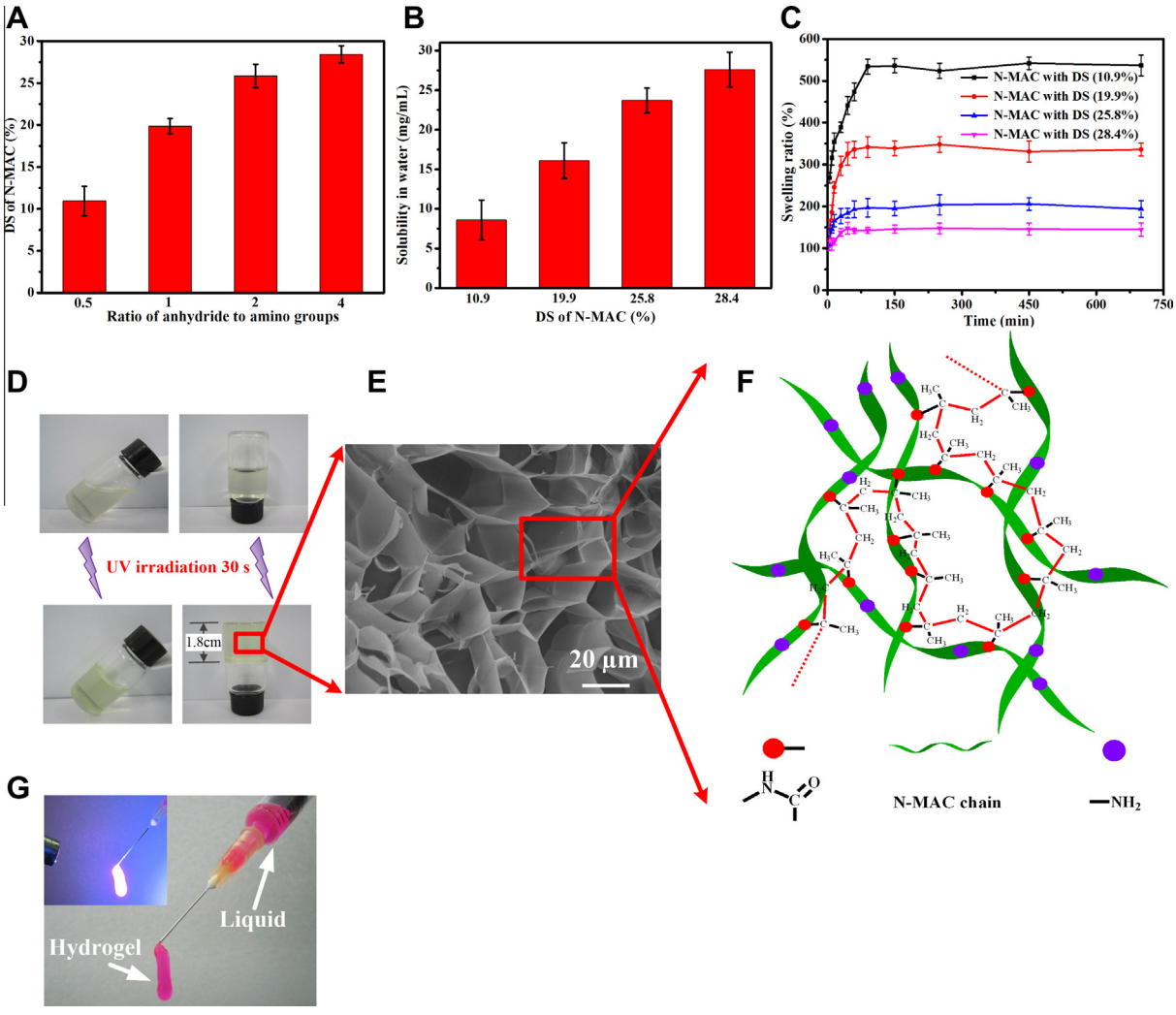

Fig. 2. Solubility, rapid UV gelation and swelling behavior of N-MAC. (A) DS of N-MAC varying with molar ratios of anhydride to amino groups. DS was positively correlated to the ratio of MA used in N-acylation reaction, which demonstrates tailor-made DS by modulating the feed ratios; (B) Solubility of N-MAC as a function of DS. Solubility of N-MAC with 28.4% DS is as high as 27.6 mg/mL in PBS; (C) Swelling ratios of N-MAC hydrogel with different DS; (D) Photos of N-MAC solution in oblique vial (upper left) and in inverted vial (upper right); N-MAC solution could form hydrogel that exhibited fixed shape respectively in oblique vial (lower left) and in inverted vial (lower right) after UV irradiation (10 mW/cm^2, 30 s). The height of as-prepared N-MAC hydrogel reached around 1.8 cm, as shown in the lower right photo; (E) ESEM photograph of N-MAC hydrogel. The sponge-like and porous structure was ascribed to high water contents; (F) Schematic presentation of the N-MAC hydrogel. Polymer networks composed of chitosan linear chains (green) were crosslinked by double bond (red), where red solid ball and blue solid ball indicated newly formed amide bond and amino group respectively; (G) The injectable N-MAC solution loaded Rhodamine B (for clear visualization) converted into hydrogel *via* syringe under 15 s UV irradiation (inset).

increasing from 10.9% to 28.4% in the ambient condition. Most importantly, the introduction of methacryloyl groups into chitosan by chemoselective N-acylation reduced the intra/intermolecular interaction and disorganized the crystalline structure of chitosan, which resulted in high solubility at neutral pH environment, such as water, PBS, glucose, SBF and DMEM.

3.2. Rapid gelation and swelling behavior of N-MAC hydrogel

Rapid gelation under the low-dose (10 mW/cm^2, 15 s) UV irradiation would be crucial to encapsulate bioactive molecules and cells with low bioactive damage, especially in the case of rapid transdermal curing hydrogel *via* injection. Here, N-MAC hydrogel was obtained *via* photopolymerization of methacryloyl carbon–carbon double bonds under low-dose UV irradiation (15 s). The rapid gelation properties of N-MAC should be largely ascribed to the content of carbon–carbon double bonds in N-MAC (a similar parameter to DS), so higher DS would result in shorter gelation time. The N-MAC showed rapid gelation behavior, which was useful for high efficient encapsulation of cells and bioactive molecules with low damage, compared with PEGDA-chitosan hydrogel [46] (15 min UV irradiation, 30 mW/cm^2), photocrosslinkable chitosan hydrogel [37] (UV radiation for 3–5 min, 160 W, 365 nm), and pluronic/chitosan hydrogels [47] (5–8 min, 120 W, 365 nm).

Fig. 2(C) shows the swelling behavior of N-MAC hydrogel with different DS. When DS increased from 10.9% to 28.4%, the hydrogels exhibited a shorter equilibrium swelling time and lower swelling ratios (from 530% to 150%) due to higher crosslinking density with higher DS. The hydrogels with DS from 10.9% to 28.4% reached equilibrium swelling in 45–90 min and maintained stable swelling ratio in 700 min, indicating that N-MAC hydrogel had outstanding dimensional stability. Thus N-MAC hydrogel holds great potential for encapsulation and culture of cells in stable hydrogel microenvironment *in vivo*, also for serving as injectable hydrogels with little dimensional deformation. Fig. 2(D) shows photos of N-MAC solution in slanted vial before (upper) and after (lower) UV irradiation. The N-MAC hydrogel with height about 1.8 cm maintained steady shape in slanted vial (lower left) and inverted vial (lower right),

which was obtained under UV irradiation (10 mW/cm^2) for 30 s. The cross-sectional ESEM image of N-MAC hydrogel is presented in Fig. 2(E). The pores of the hydrogels were irregular in shapes and the pore size was in range of 10–60 μm. The crosslinking network structure of N-MAC hydrogel is shown in Fig. 2(F). The N-MAC polymer networks were formed *via* photopolymerization of carbon–carbon double bonds (red line) between chitosan linear chains (green). The injectable N-MAC solution (15 mg/mL, fluid viscosity η = 12.8 ± 1.6 Pa s) was converted into hydrogel with a syringe after 15 s UV irradiation in Fig. 2(G), and Rhodamine B was incorporated into hydrogel for clear visualization. Rapid gelation and injectability of N-MAC provided a promising chitosan hydrogel for rapid transdermal curing hydrogel *in vivo*. The force constantly increased before 2 mm displacement, and it was broken at the displacement of 2.5 mm. We use the maximum force and contact area to calculate the compressive strength and elastic modulus. Moreover, the compressive strength and elastic modulus of N-MAC hydrogel were 2.4 ± 0.7 kPa and 11.5 ± 3.2 kPa, respectively, which is 1.9 times stronger than that of porcine skin gelatin with 5 w/v% concentration [48].

3.3. Patterned N-MAC microgel with defined size and dimension

The procedure for patterning NIH/3T3 cell-laden N-MAC microgel *via* UV lithography is illustrated in Fig. 3(A). The spatiotemporal designability approach was composed of mixing NIH/3T3 cells, prepolymer solution and I2959, sequentially applying low-dose UV irradiation with photomask prior to removing uncrosslinked solution and harvesting from substrates. Patterned N-MAC microgel with defined size and dimension (regular geometric pattern and complex microscale logos) was fabricated *via* UV lithography with help of tailor-made photomask library (Fig. 3(B)). The fluorescence images of patterned microgel, such as regular geometric pattern (top) and complex microscale logos (bottom), highly tallied with photomask library (Fig. 3(C)). The matching degree of patterned N-MAC microgel was as high as 96.3%. N-MAC microgels can be fabricated *via* UV lithography, providing advantages of rapid, robust, cost-effective and good spatialtemporal control N-MAC microgel would be fabricated via UV lithography, which had the advantages of rapid, robust, cost-effective and good spatialtemporal control [49]. Potentially, these chitosan microgels would be optimal building blocks for construction of regenerative tissues and/or organ units.

3.4. In vitro cytotoxicity of N-MAC

Since the cytocompatibility is a crucial factor in maintaining normal cells survival, proliferation and differentiation, the cytocompatibility of N-MAC solution was evaluated by the CCK-8 assay using NIH/3T3 cell line. We assessed the cytocompatibility of N-MAC in two cases. One is high concentration N-MAC in mixture of N-MAC/cell with short contact time (usually less than 30 min) before UV irradiation; and another is low concentration of remaining uncrosslinked N-MAC in N-MAC hydrogel after UV irradiation. The cell viability with concentration of 670 μg/mL and 167.5 μg/mL was 80.2 ± 2.0% at 12 h and 93.7 ± 3.8% at 48 h (Fig. 4(A)), respectively. In addition, no statistically significant differences were observed in NIH/3T3 cell viability containing N-MAC solution

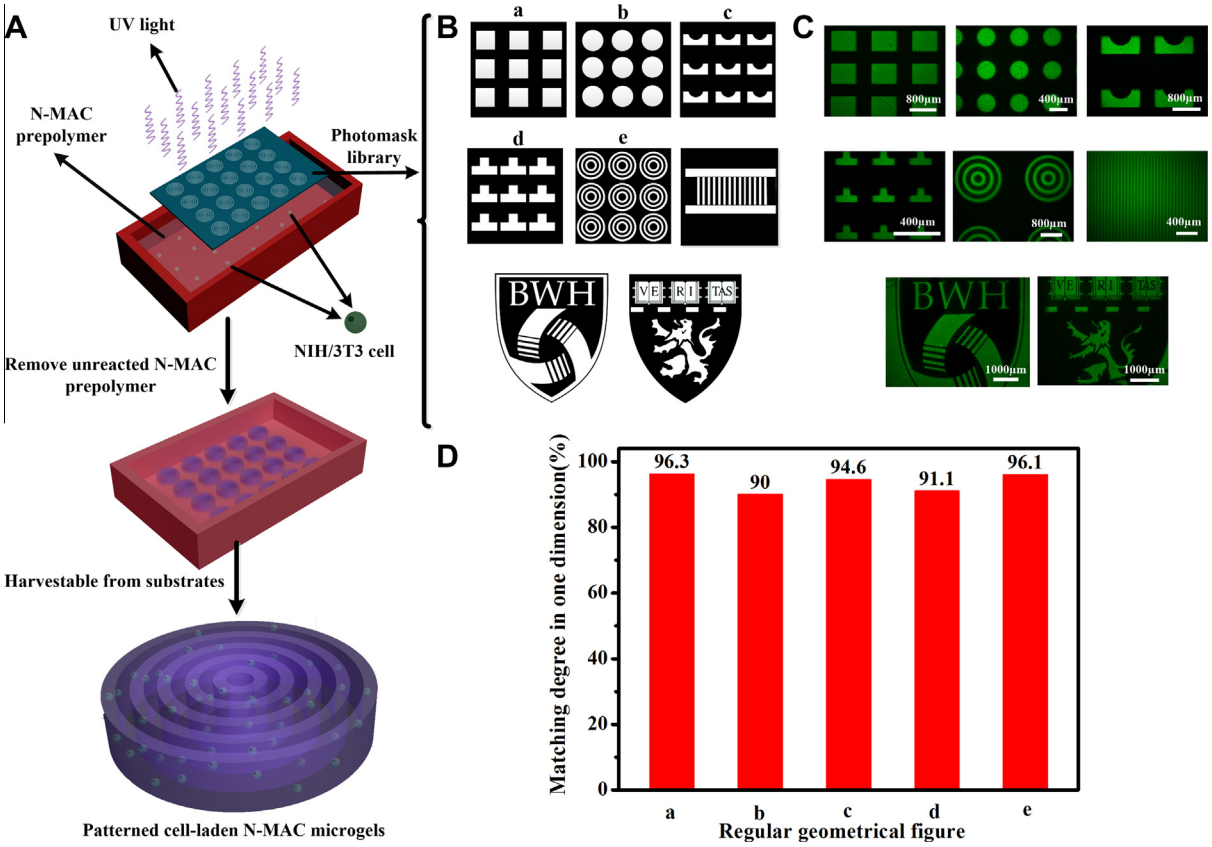

Fig. 3. Patterned N-MAC microgels with spatiotemporal designability. (A) Photolithography for *in situ* cells-laden N-MAC microgel pattern with UV exposure of 30–90 s. Patterned cell-laden N-MAC microgels were fabricated by mixing NIH/3T3 cells, N-MAC solution and I2959 followed *via* exposure to UV light; (B) Photomask library designed by AutoCAD 2007, such as regular geometric shapes (top) and complex logos (bottom); (C) Fluorescence images of N-MAC microgels using photomask library. Regular geometric shapes (top) and complex logos (down) devotedly replicated the photomask library; (D) The matching degrees between photomasks and patterned N-MAC microgels including regular geometric shapes and complex logos were ranging from 90 to 96%.

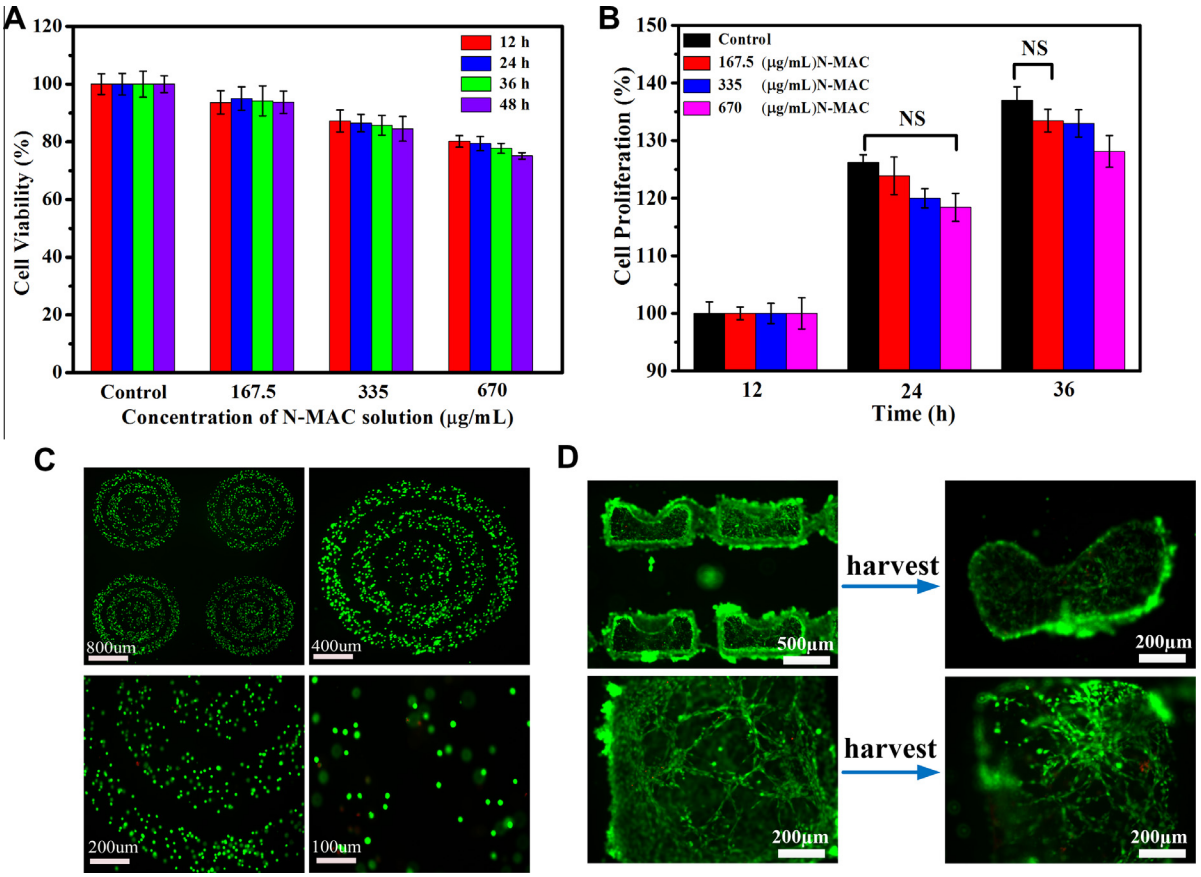

Fig. 4. Cell viability of N-MAC solution and patterned N-MAC microgels for 3D cells culture. (A) NIH/3T3 cell viability of N-MAC solution with different concentrations for culture 12, 24, 36 and 48 h, respectively, and culture medium was used as control group. Each point is presented as mean ± SD ($n = 5$, $^{*}p < 0.01$); (B) Proliferation of NIH/3T3 cells in the presence of N-MAC solution for culture 12, 24 and 36 h. Each point is presented as mean ± SD ($n = 5$); (C) Fluorescence images of live/dead (green/red) assay for NIH/3T3 cells in the patterned N-MAC microgels with concentric rings (30 s low-dose UV irradiation, after 2 days in culture). The UV photolithography showed no negative effect over the viability of the NIH/3T3 cells in patterned N-MAC microgels; (D) Fluorescence images of patterned N-MAC microgels before (left side) and after (right side) harvesting.

compared with the control group, although the average cell viability was lower than that of the control groups. Cell proliferation maintained 118.4 ± 2.5% with concentration of 670 μg/mL at 24 h and 133.0 ± 2.4% and with concentration of 167.5 μg/mL at 36 h (Fig. 4B). Notably, cell proliferation revealed that the N-MAC solution had no significantly negative effect on cell growth and proliferation, and no cytotoxic compounds were released from N-MAC solution. In addition, statistically significant differences of cell proliferation were not observed between N-MAC solution and the control group (marked by "NS"), although the average cell proliferation was lower than that of the control groups (Fig. 4(B)). More than 80% cell viability and approximate 120% cell proliferation in the N-MAC solution indicated that N-MAC was an emerging candidate for mimicking native extracellular matrix (ECM).

3.5. Patterned cell-laden N-MAC microgels

Patterned cell-laden N-MAC microgels had hold great potential for applications in tissue engineering and regenerative medicine. To investigate the cytocompatibility of the patterned N-MAC hydrogel, the viability of encapsulated NIH/3T3 cells within microgel was evaluated by live/dead staining. Fig. 4(C) shows fluorescence micrographs of patterned cells in patterned N-MAC microgels after 4 h incubation, and the cells were stained by the live/dead kit to distinguish live cells (green fluorescence) from dead ones (red fluorescence). Three green patterned concentric rings consisted of living NIH/3T3 cells that appeared under fluorescent microscope and few red fluorescence cells are observed in Fig. 4(C) with different magnifications. The patterned cells in hydrogel perfectly replicated the concentric rings pattern of photomask. The cells in N-MAC microgel exhibited cell viability as high as 96.3 ± 1.3%, which indicated good cytocompatibility of N-MAC hydrogel toward the 3T3 cell line (Fig. 4(C)). *In situ* encapsulation of NIH/3T3 cells in N-MAC microgel was patterned into concentric rings *via* UV lithography. In addition, the UV irradiation intensity (10 mW/cm^2) and time (15 s) involving in UV lithography hardly had effect on the viability of the encapsulated NIH/3T3 cells in N-MAC. The patterned cell-laden N-MAC microgel was easily harvested from substrates by cell scraper, and provided building blocks with defined size and dimension for framing 3D cell microenvironment *in vivo* and mimicking ECM (Fig. 4(D)). The microgels remained clear concavity framework for incubation 2 days both before harvesting (left) and after harvesting (right). The 3T3 fibroblasts had round morphology at day 1, and then most 3T3 fibroblasts had elongated cell morphology at day 4 and 7 [50]. The 3T3 fibroblasts had cell survival rates of approximately 90% from day 1 to day 7 without significant differences. The 3T3 fibroblasts encapsulated inside N-MAC hydrogel exhibited a spindle shape at day 2. The interconnected porous structure of microgels could provide a pathway for nutrients and oxygen. Nutrients and oxygen from the medium diffused into the hydrogel, supporting

growth and proliferation of the cells encapsulated in the hydrogels. The spatial distribution of cells in patterned N-MAC microgel was investigated by observing cell morphology in Fig. 4(D). NIH/3T3 cells were a heterogeneous distribution in the patterned microgel. Slightly more cells were located on the exterior surface of the microgel (Fig. 4(D)), which was largely due to heterogeneous nutrients and oxygen concentration distribution between the exterior surface and interior of hydrogel. For regeneration of specific tissue and/or organ *in vitro*, the harvestable patterned cell-laden microgels are deemed to be a promising strategy to encapsulate multiple-types of cells in microgels as building blocks with defined size and dimension, which can be further assembled for construction co-culture cell arrays, even the regenerative tissue units with specific physiological function. It is envisioned that the harvestable patterned cell-laden microgel with different types of cells would enable the building of heterogeneous tissues and/or organs. In addition, cell-laden polysaccharide microgels with amino groups and cohering microgels using glues (such as short DNA strand [51]) would be used to build basic architectures of native tissues.

3.6. Rapid transdermal curing N-MAC hydrogel in vivo

The UV light with wavelength of 320–400 nm has a deeper penetration into the skin and allows transdermal curing hydrogel *via* low-dose UV irradiation. Although the UV light has poor penetration to tissue, the UV light still penetrates the mice skin with 45∼52 % transmission (Fig. 5(A)). The N-MAC solution was injected into subcutaneous space of mice back through minimally invasive clinical syringe with 25G needles (left column in Fig. 5B), and sequentially applied low-dose UV irradiation with low UV intensity (10 mW/cm^2) and short UV irradiation time (60 s). Low-dose UV irradiation (10∼30 J/cm^2) means that UV exposure is applied at 100 mW/cm^2 for 100s or 300 mW/cm^2 for 100 s [52]. Curing of N-MAC hydrogel was observed by bulges on the back (Fig. 5(B)). Compared with the long gelation time (5–60 min) of previously reported injectable chitosan hydrogel including thermally-induced gelation (chitosan/β-glycerophosphate) [27,28] and pH-induced gelation [29] (chitosan/polyacrylamide), our N-MAC hydrogels required much shorter transdermal cuing time *in vivo* (60 s). For general observation transdermal curing N-MAC hydrogel *in vivo*, the injection sites were surgically dissected to expose the N-MAC hydrogel with adjacent skin (Fig. 5(C)). The N-MAC depots were tightly adhered to the injection regional skin, which indicated that the injectable N-MAC solution could rapidly convert into hydrogel with well affinity to skin *via* skin-penetrable UV crosslinking. The interface between tissue and foreign material occurs in a series of alterations in terms of changes in the microvasculature including inflammation and bleeding [53], however serious inflammatory response was hardly observed near the N-MAC hydrogel injection site in Fig. 5(C).

Low-dose UV irradiation was crucial for applying in the clinical cases [54]. Because long term UV radiation resulted in acute and chronic skin damage due to the degenerative changes in cells of skin and fibrous tissue [55,56]. For transdermal curing the N-MAC hydrogel *in vivo and* voiding skin damage, we choose low UV intensity (10 mW/cm^2) and short UV irradiation time (60 s) because cell viability still maintained high vitality at 10 mW/cm^2 with 60s UV irradiation [48]. To identify the potential skin injury induced by UV irradiation, we analyzed histological section images of the skin with and without UV irradiation in Fig. 5(D). As the cornified layer was clearly visible (no exfoliating), the epidermal cells arranged regularly, and the underlying fibroblasts maintained their random arrangement in Fig. 5D–1. Except for the occasional infiltrate of lymphocytes, no degenerative or inflammatory changes occurred and then the hair follicles did not dilate abnormally in dermis layer (Figs. 5(D)–2). No striking changes occurred in the subcutaneous tissue: elastosis (deposition of abnormal elastic fibers), collagen degeneration, dilated microvasculature in Figs. 5(D)–3. Low-dose UV irradiation hardly induced significant tissue differences in irradiated region.

To investigate the biocompatibility of N-MAC hydrogel, the *in vivo* inflammatory response to hydrogel was evaluated by H&E staining of the surrounding skin tissues at different time (Fig. 5(E)). Transdermal curing N-MAC hydrogel was indicated by eosin-staining within the subcutaneous space of mice. Usually in the organism an interface is immediately created between the implanted material and the blood, which causes a series of physiological disturbance such as evoking of inflammatory reactions including several phases: blood-material interactions, acute inflammation, chronic inflammation, foreign body reaction (FBR), and fibrous encapsulation [57]. A new interface consisting of inflammatory cells (e.g., neutrophile granulocyte) was rapidly generated between the N-MAC hydrogel and skin after injection. At 2 days, the N-MAC hydrogel resulted in abundant inflammatory cells infiltrating into the hydrogel-tissue interface (marked by yellow dotted lines in Fig. 5(E)), and inflammatory cells density and width of inflammatory region were $5641 \pm 645\ mm^{-2}$ and $338.3 \pm 46\ \mu m$ respectively. The inflammatory response to the N-MAC hydrogel significantly decreased at 5 days, suggesting a relatively mild acute inflammatory response. For example, inflammatory cell density and width of inflammatory region were $3635 \pm 664\ mm^{-2}$ (decreased by 35.6%) and $145.8 \pm 24\ \mu m$ (decreased by 56.9%), respectively. Statistically significant differences are observed in the two factors that signify inflammation: inflammatory cells density and width of inflammatory region were reduced although inflammatory cellular infiltration at the hydrogel-tissue interface is still present at this stage. As expected, acute inflammatory response after 7 days at the hydrogel-tissue interface was significantly reduced again and inflammatory cell density and width of inflammatory region were $1302 \pm 203\ mm^{-2}$ and $78.1 \pm 27\ \mu m$ respectively with slight hydrogel degradation marked by yellow arrow in Fig. 5(E) (e). The N-MAC hydrogel partially degraded (marked by two yellow arrows in Fig. 5(E) (g)) within the subcutaneous space after 10 days; and no chronic inflammation, such as foreign body giant cells, macrophages, fibrous capsules or granulation tissue, were observed in the inflammatory region. Additionally, no gaps appeared on the hydrogel-tissue interface, also suggesting evidence of regional integration between hydrogel and tissue (Fig. 5(E)). After N-MAC hydrogel injections, there were more inflammatory cells (neutrophils were abundant) than there were at later times with statistically significant difference. The N-MAC hydrogel induced only a relatively mild acute inflammatory response, giving rise to a few neutrophils and other inflammatory cells (leukocyte). Nevertheless, the amount of inflammatory cells associated with later times point was smaller, and even almost disappear, suggesting that N-MAC hydrogel stimulated a relatively slight acute inflammatory response but it cannot transform into chronic inflammation. N-MAC hydrogel could afford good biocompatibility, making them potentially promising for subcutaneous prosthesis fillers and tissue cavity fillers. Overall, the N-MAC hydrogel possesses well histocompatibility and could serve as transdermal curing depot for localized drug delivery due to no adverse inflammatory response with tissues/organs.

The representative X-ray images of mice and AOI (area of interest) are displayed in Fig. 5(G). The hydroxyapatite particles in N-MAC hydrogel could be detected clearly under X-ray photography (Fig. 5(G), labeled by yellow triangles) and were dispersed in N-MAC hydrogel uniformly *in vivo*. Hydroxyapatite plays an important role in procedure of bone formation. So it is expected that ectopic bone formation would be achieved through incorporation hydroxyapatite into N-MAC hydrogel by means of transdermal curing *in vivo*. The *in vitro* cumulative release profile of BSA from

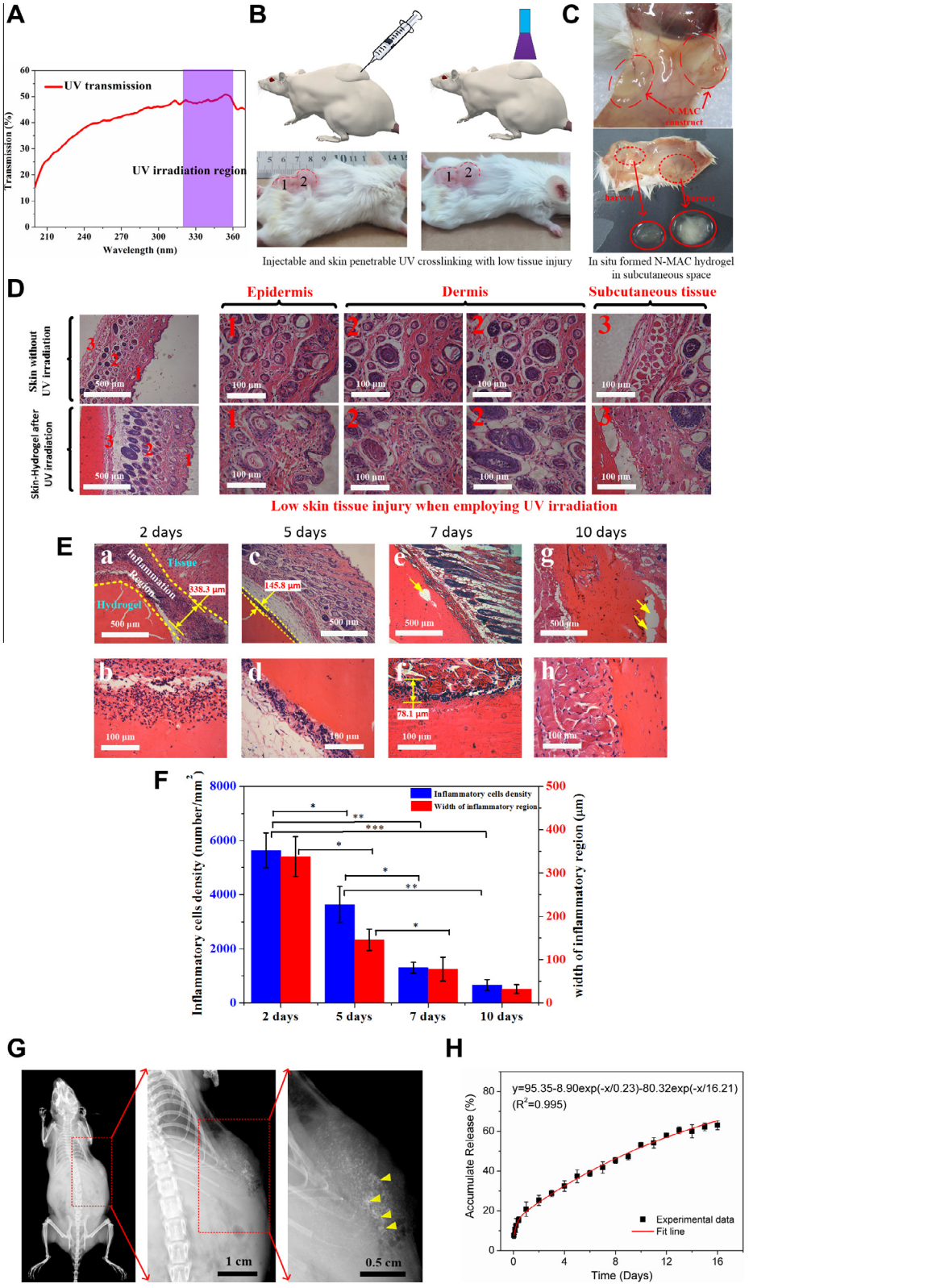

Fig. 5. Injectable and transdermal curing N-MAC *in vivo*. (A) UV transmission spectrum of mice skin. The purple bar corresponds to the wavelength region of UV irradiation lamp (320–360 nm); (B) Schematic diagram of transdermal curing of injectable N-MAC before (left) and after (right) skin-penetrable UV crosslinking; Photos of mice (bottom, after shaving back feather) with injection N-MAC solution before (left) and after (right) UV irradiation for 60 s; (C) Typical photos of N-MAC hydrogel adjacent with regional skin (up) and harvested hydrogel (down) after 6 days; (D) H&E stained histological images of subcutaneous tissue without UV irradiation (upside) and with UV irradiation (10 mW/cm^2) (underside); The number 1, 2, 3 represented different regions of skin tissue; 1: epidermis, 2: dermis, 3: subcutaneous tissue; (E) H&E stained histological images of subcutaneous tissue at 2 days (a,b), 5 days (c,d), 7 days (e,f) and 10 days (g,h); The inflammatory regions were shown with inflammatory cells (neutrophils) around injection site labeled by yellow dotted lines; (F) The inflammatory response evaluated by neutrophils density and width of inflammatory regions at different time; (G) *X*-ray images of mice with HA powder in N-MAC hydrogel; (H) *In vitro* accumulative release profiles of BSA from N-MAC hydrogel. The inset shows the mathematical equation according to the fitting curve.

N-MAC hydrogel in PBS solution within 16 days is shown in Fig. 5(H). The macromolecular drug model BSA release profile was characterized by a burst release (about 20%) within 12 h and a sustained release with a positive correlation in the following 16 days. Compared with the burst release profile of conventional thermosensitive PEG-grafted chitosan hydrogel [58], a burst release (about 52–67%) of BSA in the first 5 h, BSA release was completed in the period of 60–70 h. Injectable and UV-crosslinkable N-MAC hydrogel can localize and prolong the BSA release profile.

UV crosslinkable and injectable chitosan was *in situ* formed hydrogel *in vivo* at desired site with a spatiotemporally controlled manner under physiological condition, which can maintain the intrinsic structure and bioactivity of drugs or biomolecules during the drug uploading process, and avoid obvious pH/temperature shock in tissue milieu. The localized protein release based on UV-crosslinking N-MAC hydrogel could provide a potential strategy for *in vivo* sustained and localized release of bioactive macromolecule (e.g., polypeptide or protein, DNA, growth factor and macromolecular drug) encapsulated in hydrogel. Rapid transdermal curing chitosan hydrogel *in vivo* will reveal promising prospects for avoiding large-scale invasive implantation especially in clinical application.

4. Conclusions

Hydrosoluble, UV-crosslinkable and injectable N-MAC was synthesized by single-step highly chemoselective N-acylation reaction between amino groups and the methacrylate groups. The introduction of methacryloyl groups into chitosan led to significant increasing of solubility in neutral pH environment. The cell viability in N-MAC hydrogel maintained 96.3 ± 1.3%. Serving as chitosan based building blocks for bottom-up tissue engineering, patterned cell-laden and highly matching degree N-MAC microgels were fabricated with low-dose UV irradiation (10 mW/cm^2, 15 s). The *in vivo* inflammatory analysis indicated that low-dose UV irradiation hardly induced skin injury and acute inflammatory response disappeared after 7 days. Rapid transdermal curing N-MAC hydrogels *in vivo* are potentially applied in localized drug delivery with minimally invasive clinical surgery and can prolong release behavior of therapeutic drugs. This hydrosoluble, UV-crosslinkable and injectable chitosan would allow rapid, robust and cost-effective fabrication of patterned cell-laden polysaccharide microgels with unique amino groups serving as building blocks for tissue engineering, rapid transdermal curing hydrogel *in vivo* for localized and sustained drug delivery.

5. Conflict of interest

The authors declare no conflicts of interest.

Acknowledgements

The authors thank the financial support from National Science Foundation of China (51372051, 51321061, 11372243), National Basic Science Research Program (2012CB339300), State Key Laboratory of Urban Water Resource and Environment of Harbin Institute of Technology (2013TS09), Innovation Talents of Harbin Science and Engineering (2013RFLXJ023) and Fundamental Research Funds for Central Universities (HIT.IBRSEM.201302). F.X. was supported by the National 111 Project of China (B06024) and International Science & Technology Cooperation Program of China (2013DFG02930).

Appendix A. Figures with essential color discrimination

Certain figures in this article, particularly Figs. 1–5, are difficult to interpret in black and white. The full color images can be found in the on-line version, at http://dx.doi.org/10.1016/j.actbio.2015.04.026

References

[1] Lutolf MP, Hubbell JA. Synthetic biomaterials as instructive extracellular microenvironments for morphogenesis in tissue engineering. Nat Biotechnol 2005;23:47–55.
[2] Ott HC, Matthiesen TS, Goh SK, Black LD, Kren SM, Netoff TI, et al. Perfusion-decellularized matrix: using nature's platform to engineer a bioartificial heart. Nat Med 2008;14:213–21.
[3] Place ES, Evans ND, Stevens MM. Complexity in biomaterials for tissue engineering. Nat Mater 2009;8:457–70.
[4] Petersen TH, Calle EA, Zhao LP, Lee EJ, Gui LQ, Raredon MB, et al. Tissue-engineered lungs for in vivo implantation. Science 2010;329:538–41.
[5] Dvir T, Timko BP, Kohane DS, Langer R. Nanotechnological strategies for engineering complex tissues. Nat Nanotechnol 2011;6:13–22.
[6] Bajaj P, Schweller RM, Khademhosseini A, West JL, Bashir R. 3D biofabrication strategies for tissue engineering and regenerative medicine. Annu Rev Biomed Eng 2014;16:247–76.
[7] Elbert DL. Bottom-up tissue engineering. Curr Opin Biotechnol 2011;22:674–80.
[8] Khademhosseini A, Langer R. Microengineered hydrogels for tissue engineering. Biomaterials 2007;28:5087–92.
[9] Hahn MS, Miller JS, West JL. Three-dimensional biochemical and biomechanical patterning of hydrogels for guiding cell behavior. Adv Mater 2006;18:2679–84.
[10] Zorlutuna P, Jeong JH, Kong H, Bashir R. Stereolithography-based hydrogel microenvironments to examine cellular interactions. Adv Funct Mater 2011;21:3642–51.
[11] Tasoglu S, Kavaz D, Gurkan UA, Guven S, Chen P, Zheng RL, et al. Paramagnetic levitational assembly of hydrogels. Adv Mater 2013;25:1137–43.
[12] McCain ML, Agarwal A, Nesmith HW, Nesmith AP, Parker KK. Micromolded gelatin hydrogels for extended culture of engineered cardiac tissues. Biomaterials 2014;35:5462–71.
[13] Mironov V, Visconti RP, Kasyanov V, Forgacs G, Drake CJ, Markwald RR. Organ printing: tissue spheroids as building blocks. Biomaterials 2009;30:2164–74.
[14] Villar G, Graham AD, Bayley H. A tissue-like printed material. Science 2013;340:48–52.
[15] DeForest CA, Polizzotti BD, Anseth KS. Sequential click reactions for synthesizing and patterning three-dimensional cell microenvironments. Nat Mater 2009;8:659–64.
[16] Jeong JH, Chan V, Cha C, Zorlutuna P, Dyck C, Hsia KJ, et al. "Living" microvascular stamp for patterning of functional neovessels; orchestrated control of matrix property and geometry. Adv Mater 2012;24:58–63.
[17] Gurkan UA, Fan Y, Xu F, Erkmen B, Urkac ES, Parlakgul G, et al. Simple precision creation of digitally specified, spatially heterogeneous, engineered tissue architectures. Adv Mater 2013;25:1192–8.
[18] Fukuda J, Khademhosseini A, Yeo Y, Yang XY, Yeh J, Eng G, et al. Micromolding of photocrosslinkable chitosan hydrogel for spheroid microarray and co-cultures. Biomaterials 2006;27:5259–67.
[19] Karp JM, Yeo Y, Geng WL, Cannizarro C, Yan K, Kohane DS, et al. A photolithographic method to create cellular micropatterns. Biomaterials 2006;27:4755–64.
[20] Obara K, Ishihara M, Fujita M, Kanatani Y, Hattori H, Matsui T, et al. Acceleration of wound healing in healing-impaired db/db mice with a photocrosslinkable chitosan hydrogel containing fibroblast growth factor-2. Wound Repair Regen 2005;13:390–7.
[21] Fujita M, Ishihara M, Morimoto Y, Simizu M, Saito Y, Yura H, et al. Efficacy of photocrosslinkable chitosan hydrogel containing fibroblast growth factor-2 in a rabbit model of chronic myocardial infarction. J Surg Res 2005;126:27–33.
[22] Tan HP, Marra KG. Injectable, biodegradable hydrogels for tissue engineering applications. Materials 2010;3:1746–67.
[23] Ko DY, Shinde UP, Yeon B, Jeong B. Recent progress of in situ formed gels for biomedical applications. Prog Polym Sci 2013;38:672–701.
[24] Jiang T, Deng M, James R, Nair LS, Laurencin CT. Micro- and nanofabrication of chitosan structures for regenerative engineering. Acta Biomater 2014;10:1632–45.
[25] Anitha A, Sowmya S, Kumar PTS, Deepthi S, Chennazhi KP, Ehrlich H, et al. Chitin and chitosan in selected biomedical applications. Prog Polym Sci 2014;39:1644–67.
[26] Ta HT, Dass CR, Dunstan DE. Injectable chitosan hydrogels for localised cancer therapy. J Controlled Release 2008;126:205–16.
[27] Chenite A, Chaput C, Wang D, Combes C, Buschmann MD, Hoemann CD, et al. Novel injectable neutral solutions of chitosan form biodegradable gels in situ. Biomaterials 2000;21:2155–61.
[28] Ruel-Gariepy E, Shive M, Bichara A, Berrada M, Le Garrec D, Chenite A, et al. A thermosensitive chitosan-based hydrogel for the local delivery of paclitaxel. Eur J Pharm Biopharm 2004;57:53–63.

[29] Mukhopadhyay P, Sarkar K, Bhattacharya S, Bhattacharyya A, Mishra R, Kundu PP [pH sensitive N-succinyl chitosan grafted polyacrylamide hydrogel for oral insulin delivery]. Carbohydr Polym 2014;112:627–37.
[30] Ifkovits JL, Burdick JA. Review: photopolymerizable and degradable biomaterials for tissue engineering applications. Tissue Eng 2007;13:2369–85.
[31] Zhang Y, Zhan F, Shi WF. Photopolymerization behavior and properties of highly branched poly(thioether-urethane) acrylates used for UV-curing coatings. Prog Org Coat 2011;71:399–405.
[32] Woranuch S, Yoksan R. Preparation, characterization and antioxidant property of water-soluble ferulic acid grafted chitosan. Carbohydr Polym 2013;96:495–502.
[33] Wang Z, Zeng R, Tu M, Zhao J. Synthesis, characterization of biomimetic phosphorylcholine-bound chitosan derivative and in vitro drug release of their nanoparticles. J Appl Polym Sci 2013;128:153–60.
[34] Shi B, Shen Z, Zhang H, Bi J, Dai S. Exploring N-imidazolyl-O-carboxymethyl chitosan for high performance gene delivery. Biomacromolecules 2012;13:146–53.
[35] Huang SJ, Sun SL, Chiu CC, Wang LF. Retinol-encapsulated water-soluble succinated chitosan nanoparticles for antioxidant applications. J Biomater Sci Polym Ed 2013;24:315–29.
[36] Ono K, Saito Y, Yura H, Ishikawa K, Kurita A, Akaike T, et al. Photocrosslinkable chitosan as a biological adhesive. J Biomed Mater Res 2000;49:289–95.
[37] Valmikinathan CM, Mukhatyar VJ, Jain A, Karumbaiah L, Dasari M, Bellamkonda RV. Photocrosslinkable chitosan based hydrogels for neural tissue engineering. Soft Matter 2012;8:1964–76.
[38] Gao X, Zhou Y, Ma G, Shi S, Yang D, Lu F, et al. A water-soluble photocrosslinkable chitosan derivative prepared by Michael-addition reaction as a precursor for injectable hydrogel. Carbohydr Polym 2010;79:507–12.
[39] Ma G, Liu Y, Kennedy JF, Nie J. Synthesize and properties of photosensitive organic solvent soluble acylated chitosan derivatives (2). Carbohydr Polym 2011;84:681–5.
[40] Zhou Y, Ma G, Shi S, Yang D, Nie J. Photopolymerized water-soluble chitosan-based hydrogel as potential use in tissue engineering. Int J Biol Macromol 2011;48:408–13.
[41] Qi ZQ, Xu J, Wang ZL, Nie J, Ma GP. Preparation and properties of photo-crosslinkable hydrogel based on photopolymerizable chitosan derivative. Int J Biol Macromol 2013;53:144–9.
[42] Dash M, Chiellini F, Ottenbrite RM, Chiellini E. Chitosan—A versatile semi-synthetic polymer in biomedical applications. Prog Polym Sci 2011;36:981–1014.
[43] Naik S, Bhattacharjya G, Talukdar B, Patel Bhisma K. Chemoselective acylation of amines in aqueous media. Eur J Org Chem 2004;2004:1254–60.
[44] Monier M, Wei Y, Sarhan AA, Ayad DM. Synthesis and characterization of photo-crosslinkable hydrogel membranes based on modified chitosan. Polymer 2010;51:1002–9.
[45] Bangyekan C, Aht-Ong D, Srikulkit K. Preparation and properties evaluation of chitosan-coated cassava starch films. Carbohydr Polym 2006;63:61–71.
[46] Ma GP, Zhang XD, Han J, Song GQ, Nie J. Photo-polymeriable chitosan derivative prepared by Michael reaction of chitosan and polyethylene glycol diacrylate (PEGDA). Int J Biol Macromol 2009;45:499–503.
[47] Lee JI, Kim HS, Yoo HS. DNA nanogels composed of chitosan and Pluronic with thermo-sensitive and photo-crosslinking properties. Int J Pharm 2009;373:93–9.
[48] Lin RZ, Chen YC, Moreno-Luna R, Khademhosseini A, Melero-Martin JM. Transdermal regulation of vascular network bioengineering using a photopolymerizable methacrylated gelatin hydrogel. Biomaterials 2013;34:6785–96.
[49] Williams CG, Malik AN, Kim TK, Manson PN, Elisseeff JH. Variable cytocompatibility of six cell lines with photoinitiators used for polymerizing hydrogels and cell encapsulation. Biomaterials 2005;26:1211–8.
[50] Wu J, Ding Q, Dutta A, Wang Y, Huang YH, Weng H, et al [An injectable extracellular matrix derived hydrogel for meniscus repair and regeneration]. Acta Biomater 2015;16:49–59.
[51] Qi H, Ghodousi M, Du Y, Grun C, Bae H, Yin P, et al [DNA-directed self-assembly of shape-controlled hydrogels]. Nat Commun 2013;4:2275.
[52] Liu ZR, Chen HL, Yang HL, Liang J, Li XM [Low-Dose UVA Radiation-Induced Adaptive Response in Cultured Human Dermal Fibroblasts]. Int J Photoenergy 2012;2012:167425.
[53] Rihova B. Immunocompatibility and biocompatibility of cell delivery systems. Adv Drug Delivery Rev 2000;42:65–80.
[54] Clydesdale GJ, Dandie GW, Muller HK. Ultraviolet light induced injury: Immunological and inflammatory effects. Immunol Cell Biol 2001;79:547–68.
[55] Ichihashi M, Ueda M, Budiyanto A, Bito T, Oka M, Fukunaga M, et al. UV-induced skin damage. Toxicology 2003;189:21–39.
[56] Matsumura Y, Ananthaswamy HN. Toxic effects of ultraviolet radiation on the skin. Toxicol Appl Pharmacol 2004;195:298–308.
[57] Anderson JM. Biological responses to materials. Annu Rev Mater Res 2001;31:81–110.
[58] Bhattarai N, Ramay HR, Gunn J, Matsen FA, Zhang MQ. PEG-grafted chitosan as an injectable thermosensitive hydrogel for sustained protein release. J Controlled Release 2005;103:609–24.